Optimization of a single defect photonic crystal laser cavity

Walter R. Frei and H. T. Johnson[a)]
Department of Mechanical Science and Engineering, University of Illinois at Urbana-Champaign, Urbana, Illinois 61801, USA

Kent D. Choquette
Department of Electrical and Computer Engineering, University of Illinois at Urbana-Champaign, Urbana, Illinois 61801, USA

(Received 29 June 2007; accepted 30 November 2007; published online 5 February 2008)

Using nonlinear programing and the geometry projection method, the quality factor of the monopole mode of a single defect photonic crystal laser cavity is improved from 38 000 to 87 000. Beginning with a design that considers only round air holes shifted away from the cavity, the radius of the nearest neighbor and of the surrounding air holes are optimized while satisfying a constraint on the resonant frequency. The total reflectivity of the photonic crystal laser structure is then defined, and it is shown that this quantity correlates strongly to the total quality factor. The reflectivity of the structure is improved by altering the shape of the holes immediately surrounding the cavity, thus leading to an improvement in quality factor. The geometry projection method is used to define the shape of the holes and the finite element and adjoint methods are used to compute the objective function and sensitivities required by the optimizer. This work demonstrates one way to optimize the Q factor of a photonic crystal laser by altering the hole shape. © *2008 American Institute of Physics*. [DOI: 10.1063/1.2838173]

INTRODUCTION

Single defect photonic crystal laser (PCL) cavities employ a defect in a regular pattern of air holes etched into a thin freestanding dielectric slab to strongly confine light into a cavity region.[1] The PCL is a promising device due to its small laser cavity mode volume and high Q factor.[2,3] The defect is usually formed by leaving a single hole unetched and changing the hole positions and radii immediately surrounding the cavity, the so-called nearest neighbor holes.[4] The effects of nearest neighbor hole radius on the Q factor have been limited to parameter searches via the finite difference time domain (FDTD) method.[5–9] Other works have shown that the nearest neighbor holes need not be circular; elliptical[10] and half-moon[11] shaped holes as well as an elongation along one axis[12] all result in high Q-factor structures. Indeed, random disorder is known to improve the Q factor of certain types of cavities.[13] The surrounding air hole lattice need not even have a periodic pattern; circular photonic crystal patterns[14,15] and quasiperiodic patterns[16] can also create an effective optical confinement. It is clear that various types of defects can improve the Q factor and that this design space has not yet been fully investigated.

This work uses the method of moving asymptotes (MMAs),[17] a gradient based optimization algorithm, to improve the Q factor of the monopole mode of a single defect PCL by altering the shape of the nearest neighbor holes. The shape of these holes is described via the geometry projection method (GPM). The GPM uses the intersection of a level plane with a three-dimensional surface fitted through a set of control points to define the hole pattern. The optimization problem can thus be defined with respect to the heights of these control points. The GPM was originally developed for structural optimization[18] and was recently applied to photonics problems.[19] The Q factor of the PCL is computed by the finite element (FE) method[20] and the sensitivities required by the MMA are computed by the adjoint method.[21]

A simple parameter search over nearest neighbor hole radius and surrounding hole radius is used first to find a starting condition with a high Q factor. This parameter search considers an additional constraint: the frequency of the resonant mode is fixed. This constraint is satisfied by rescaling the thickness of the structure. Next, the total reflectivity of the PCL structure is defined, and it is shown that an improvement in reflectivity correlates with an improvement in Q factor. The case with the highest Q factor with respect to these two parameters is used as a starting condition for the MMA. The MMA then improves the reflectivity by altering the hole shape and thus improves the Q factor.

COMPUTING THE *Q* FACTOR

The Q factor of the monopole mode of a PCL is calculated here by the FE method. Although the FE method requires more computational resources than the commonly used FDTD method, it has one significant advantage: it can easily be extended to compute material sensitivities via the adjoint method. Computing these material sensitivities is a requirement of the GPM optimization algorithm used later. The commercial package COMSOL is used for all calculations. The present work is the first application of the FE method in calculating the Q factor of a PCL.

The FE model used is shown in Fig. 1. Since the monopole mode and the structure are symmetric about the x-y plane and sixfold symmetric in the plane, only a small slice of the entire structure needs to be modeled. The PCL being

[a)]Electronic mail: htj@uiuc.edu.

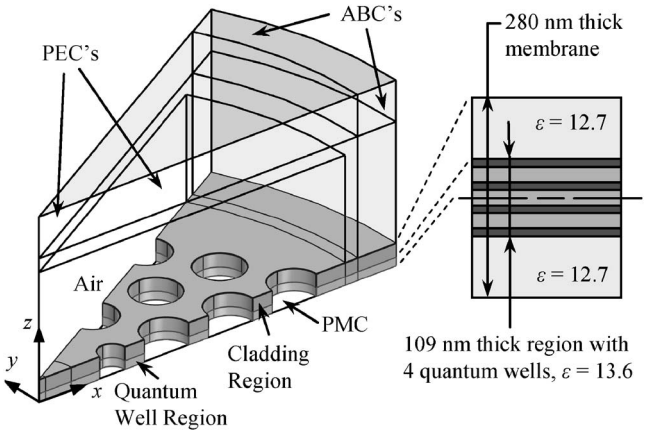

FIG. 1. The finite element model used to calculate the Q factor. Only four rows of holes are shown here for clarity; six rows of holes are used in all calculations.

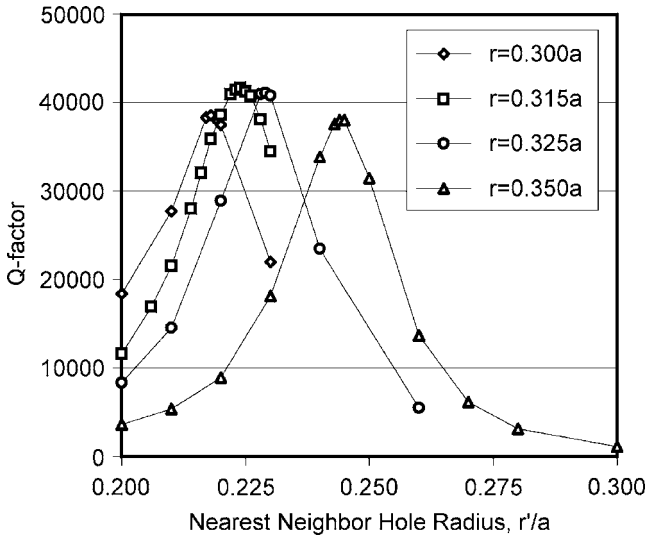

FIG. 2. The Q factor as a function of nearest neighbor hole radius r'/a for various choices of surrounding hole radius r/a. The parameter search is refined via the interval bisection near the peak. The thickness of the slab is adjusted such that the computed resonant frequency satisfies the constraint $(t/a)(a/\lambda_{\text{resonant}})=0.188$.

optimized is composed of four epitaxially grown InGaAsP quantum wells with a cladding region above and below. This structure has an emission peak at 1488.5 nm and primarily emits light with the electric fields polarized parallel to the plane of the slab. The dielectric slab is modeled using two different domains, an inner domain, with dielectric $\varepsilon=13.6$ representing the quantum well active regions, and an outer domain, $\varepsilon=12.7$ representing the cladding. These properties are found by linear interpolation.[22] The remainder of the domain is air, with $\varepsilon=1$. Perfectly electrically conducting boundary conditions are applied to the vertical symmetry planes of the domain and a perfectly magnetically conducting boundary condition is applied to the bottom symmetry plane. The remaining boundaries, to free space, are modeled using an absorbing boundary condition (ABC). If the ABC is placed far enough away from the slab, then spurious reflections from the ABC are minimized. The ABC is placed here a half wavelength away from the surface of the PCL. The structure is meshed using second order vector elements; mesh refinement studies show that the element size and order are sufficiently accurate. The maximum element size used anywhere in the domain is $\lambda/4n$, where n is the local refractive index; the total number of degrees of freedom is approximately 100 000.

The Q factor is $Q=2\pi fU/P$, where U is the integral of the time averaged total energy stored within the calculation domain, P is the integral of the power leaving the domain, and f is the frequency at resonance. The fields at resonance and the resonant frequency are found by solving an eigenvalue problem.

FINDING AN INITIAL CONDITION FOR THE OPTIMIZATION

The MMA optimization algorithm used here requires an initial condition or a PCL hole pattern from which to start the optimization. Although any initial condition could be used, it is reasonable to first use a conventional approach and then to make further improvements via the GPM method, described later.

The conventional approach to optimizing the Q factor of a PCL is to choose several evenly spaced values of the nondimensional slab thickness t/a, the nearest neighbor hole radius r'/a, and the surrounding hole radius r/a to find the best combination.[9] Although this approach is simple to implement, it offers no control over the resonant frequency of the cavity. An improved approach is used here. Since the desired output wavelength of the PCL is known, as well as the actual thickness of the slab, the nondimensional slab thickness is constrained. At resonance, the following relationship must hold:

$$\frac{t_{\text{actual}}}{\lambda_{\text{desired}}}=\frac{t}{a}\frac{a}{\lambda(t)}, \tag{1}$$

where λ_{desired} corresponds to the wavelength at the desired resonance and $a/\lambda(t)$ is a function of both the slab thickness and the hole pattern and can only be found by solving the eigenvalue problem described above.

The parameter studies done here all rescale the nondimensional thickness to satisfy the constraint of Eq. (1). The model is solved and, based on the computed a/λ, the nondimensional thickness t/a is adjusted such that the constraint is approached; this is repeated until the constraint is satisfied to within a tolerance of $\pm 0.0001t/\lambda$.

Parameter studies of the nearest neighbor hole radius r'/a and the nominal hole radius r/a are presented in Figs. 2 and 3 for a structure with a total of six rows of holes. All points satisfy the condition that $t/\lambda=280$ nm/1488.5 nm. The different curves are for different r/a. All the curves exhibit the same trend—a sharp peak in Q factor as a function of r'/a. The peaks of the curves are found via a simple bisection search. The authors are not aware of any other works that study these peaks in such detail or that consider the constraint on resonant frequency. The maximum Q factor of $\approx 42\,000$ occurs at $r/a=0.315$ and $r'/a=0.224$. Figure 3 plots the maximum Q factor as a function of r/a, that is,

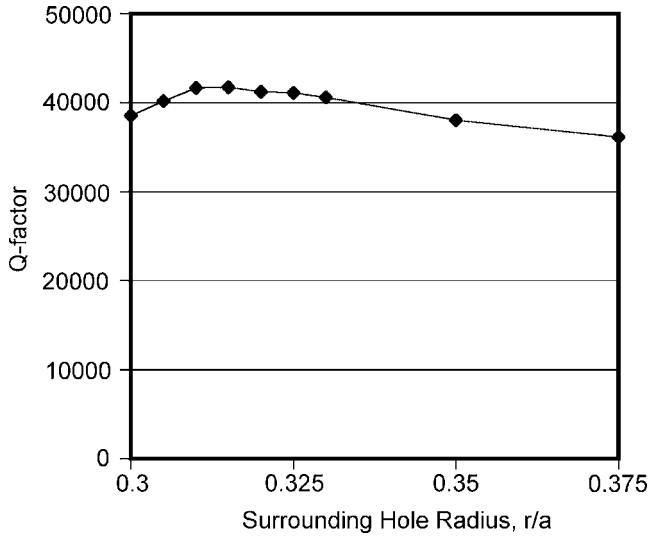

FIG. 3. The maximum Q factor as a function of surrounding hole radius r/a. The nearest neighbor hole radius r'/a at each point is shown in Fig. 2. The function does not have a sharp peak; a peak Q factor of over 40 000 is found for $r/a \approx 0.31-0.33$.

each point in this plot represents a parameter space search over r'/a, and satisfies the constraint of thickness given by Eq. (2).

Figure 2 shows that the Q factor is a strong function of the nearest neighbor hole radius, while Fig. 3 shows that the Q factor is only a weak function of the surrounding hole radius. Since the magnitudes of the fields decay rapidly away from the cavity, it makes sense that the shape of the nearest neighbor hole has the greatest effect on the Q factor. Thus, it is most reasonable to optimize the shape of the nearest neighbor hole.

This study demonstrates both the advantages and disadvantages of the parameter space search method. Searching over a small range of r'/a is simple and very straightforward to implement, but satisfying the thickness constraint still requires tens of model solutions to find the optimum r'/a for a particular choice of r/a. Searching over r/a increases the number of solutions by almost an order of magnitude since the search over r'/a must be repeated for each r/a. However, there is no particular reason to assume that this choice of parameter space, r'/a and r/a, is optimal. The choice of parameter space limits the final design to round holes, but it is known that the holes need not be round. The GPM that is used in the next section relaxes almost all constraints on the shape of the holes, but it does not directly optimize the Q factor, rather, the total reflectivity is optimized which leads to an improvement in Q factor.

CORRELATING Q FACTOR WITH REFLECTIVITY

The Q factor of a PCL is a function of cavity material properties and cavity geometry. For complex three-dimensional structures, there are no simple ways to calculate it without solving a computational model. However, there are some trends that can be predicted from simpler models of lasers. For instance, the Q factor of a simple one-dimensional laser cavity model[23] is

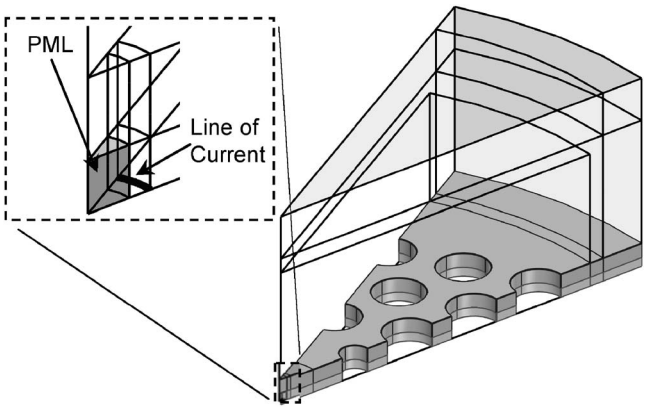

FIG. 4. The finite element model used to calculate the total reflectivity. The model has the same boundary conditions and material properties as the model used to calculate the Q factor, but it has a PML region in the center, a line of current around the PML.

$$Q = \frac{2\pi nd}{\lambda} \frac{(R_1R_2)^{1/4}}{1-(R_1R_2)^{1/2}}, \tag{2}$$

where n is the refractive index inside the cavity, λ is the wavelength at resonance, d is the length of cavity, and R_1 and R_2 are the reflectivities of the mirrors on each side of the cavity. The material properties n, size d, and lasing wavelength λ of the cavity are assumed for the moment to be fixed. Under this assumption, only the reflectivity of the mirrors surrounding the cavity can improve the Q factor. Although this equation applies only to one-dimensional laser cavities with a fixed mirror reflectivity and a well defined boundary between the cavity and the mirrors, the trends predicted by this model should similarly apply to PCL cavities. That is, an increase in reflectivity, optical confinement, must lead to an increase in Q factor.

The reflectivity of a structure is a measure of how much of the energy incident upon the structure from a certain direction, and at a certain frequency, is reflected back toward the source. That is, it quantifies the optical confinement. The reflectivity of a PCL cavity is not a quantity that can be measured experimentally but is defined here via the FE model shown in Fig. 4, which is identical to the model used to calculate the Q factor with three exceptions. First, the reflectivity model includes a perfectly matched layer (PML) in the center of the PCL structure. This material acts as an absorber: any light reflected back into the center will be almost completely absorbed. The second difference is that this model includes a source term. Immediately surrounding the central PML region, a line of constant current is applied to one edge. This source term mimics the emission from the quantum well regions: the fields produced by this line of current have the appropriate in-plane polarization and overlap the shape of the expected monopole mode. The quantum wells emit primarily TE polarized light, and the electric fields of the monopole mode are already known to be aligned with the emission from the quantum wells. The fields induced by the line of current used here are a good approximation to the fields at resonance. The last difference in this FE model is that the solutions are found from a forced excitation, rather than an eigenvalue, solution. The reflectivities

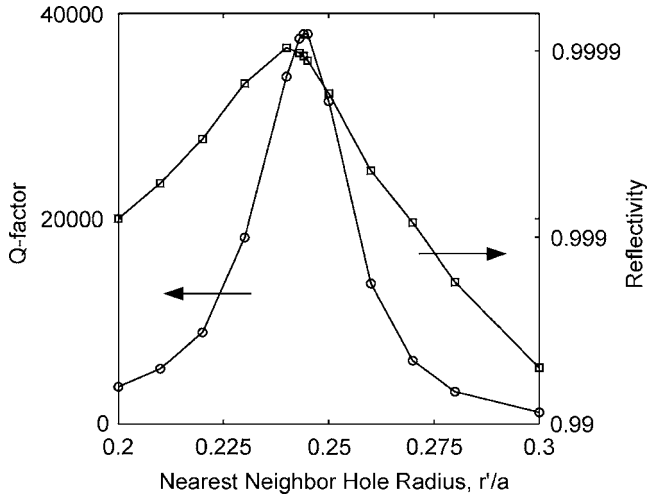

FIG. 5. The Q factor and total structural reflectivity as a function of nearest neighbor holes for a structure with surrounding hole radius of $r/a=0.35$. The structural reflectivity and Q factor exhibit the same trends.

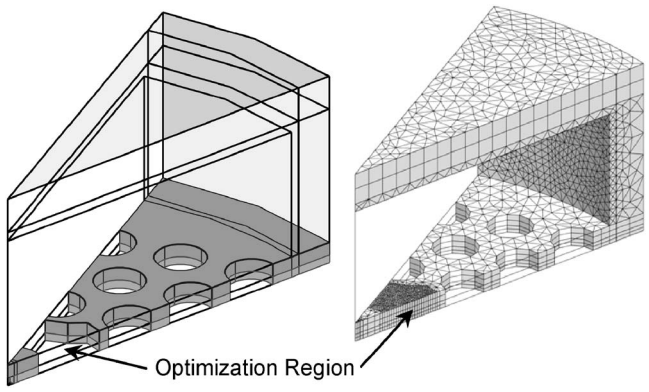

FIG. 6. The finite element model used for reflectivity optimization (left) and the mesh used (right). Some elements are removed for clarity.

are calculated at the resonant frequency of the structure, as computed by the previous model. The reflectivity is computed by integrating the Poynting vector over the boundaries to free space or the power leaving the structure, i.e., the transmittance T. The reflectivity is $R=1-T$.

The qualitative relationship between the Q factor and reflectivity is shown in Fig. 5. The Q factor and the total reflectivity are plotted as a function of nearest neighbor hole radius for a structure with surrounding hole radius of $r/a=0.35$. The reflectivity is calculated at the frequencies of the resonant mode. Although they do not correlate exactly, the curves do exhibit the same trend, thus verifying that an increase in reflectivity should lead to an increase in Q factor.

OPTIMIZING Q FACTOR VIA THE GPM

The objective of the optimization problem solved here is to increase the total reflectivity at the resonant frequency of the monopole mode by altering the hole shape. This problem is complicated by the fact that as the holes are altered to improve the reflectivity, it is possible to shift the frequency of the resonant mode of the structure. A strategy to address this is introduced. The FE model used in the optimization is identical to the model used above to compute reflectivity except that it uses a different mesh and has an optimization region in which the material properties are defined by the GPM.

The FE model and mesh used in the optimization are shown in Fig. 6. The optimization domain, an arbitrary region around the nearest neighbor hole but not intersecting the next row of holes, is meshed with triangular prismatic elements of maximum size of $a/24$. The dielectric properties in the optimization region are defined via the GPM, using a square grid of control points with spacing of $a/10$. The implementation of the GPM used here is identical to that previously presented by the authors.[19] The remainder of the slab is also meshed with triangular prismatic elements. The surrounding air is meshed with tetrahedral elements. There are four elements through the thickness of the slab. At this mesh density, there are almost 500 000 degrees of freedom in the complete model. Solving a forced excitation problem of this size using the direct linear equation solver in COMSOL on a 64 bit processor (1.8 GHz Opteron 265) takes about 1 h and requires around 6 Gbytes of random access memory.

The objective of the optimization problem is to increase total reflectivity or to increase the amount of energy that is reflected back into the cavity region. To increase the Q factor, the reflectivity must be improved at the frequency of the resonant mode, which is not directly controlled during the optimization. However, by optimizing the normalized reflectivity at several frequencies around the resonant mode of the initial structure, it is observed that the resonant mode does not shift significantly. Increasing the reflectivity is equivalent to reducing the transmittance, which can be normalized with respect to the transmittance of the initial structure. The optimization problem is thus

$$\min_{\mathbf{q}} \sum_{i} P(\mathbf{q},f_i)/P_0(f_i), \tag{3}$$

where P_0 is the transmitted power of the initial structure at the ith frequency f_i, P is the transmitted power of the optimized structure, and $\mathbf{q}$ are the heights of the control points used by the GPM to define the dielectric distribution in the optimization domain. This problem is solved by the MMA, and the problem is considered converged when the change in the objective function is less than 0.0001 between iterations.

Starting with the design achieved by the parameter space search performed above, the total reflectivity is improved by altering the hole pattern via the GPM. The initial design has a nearest neighbor hole radius of $r'/a=0.244$, a hole radius of $r/a=0.315$, and a nondimensional thickness of $t/a=0.618$. The resonant mode of this structure is at $\omega a/2\pi c=0.304$. The normalized transmitted power is minimized at $\omega a/2\pi c=0.300, 0.305, 0.310$.

The improved shape of the nearest neighbor holes and the magnitude of the z component of the magnetic field is plotted for the initial and optimized structure in Fig. 7. By improving the total reflectivity, the Q factor is more than doubled, from $\approx$38 000 to $\approx$87 000. Although the optimization is run at a constant nondimensional thickness using a material distribution defined by the GPM, an additional veri-

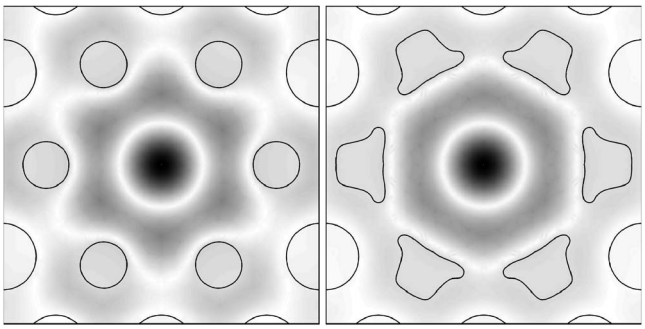

FIG. 7. The magnitude of the H_z fields of the (left) unoptimized and (right) optimized designs.

fication step is introduced that interprets the GPM data and adjusts the thickness of the slab such that the constraint of Eq. (1) is satisfied.

Figure 7 shows the magnitude of the H_z fields for the unoptimized and optimized designs. The fields are more strongly confined in the optimized design. This may be due to the broadening of the interface between dielectric and air; looking outward from the center, the location of the interface is brought closer. This two-dimensional plot of the fields does not capture the full complexity of the three-dimensional solution, but the approximate improvements are illustrated reasonably well in this cross-sectional view.

The designs as defined by the GPM are verified by creating a new FE model using the level set curves that delineate the material boundaries. This verification FE model is identical to the model used above to calculate the Q factor; it varies only in the shape of the nearest neighbor holes. The level set curves are used to create geometry that can be meshed using conformal elements rather than the fine mesh used by the optimization FE model. This significantly speeds up the verification calculation. There is an error of approximately 10% introduced into the calculations by this interpretation. There is also some imprecision introduced when converting the level set curves of the GPM into the nonuniform rational B-spline (NURBS) surface definitions used by COMSOL. The nondimensional thickness t/a of this model is iteratively adjusted, as described above to satisfy the constraint on resonant frequency. The thickness is adjusted between $t/a=0.618$ and 0.622, a negligible change which indicates that the strategy discussed above effectively minimizes the frequency shift of the resonant mode.

The total computed Q factor of a PCL is often divided into two components: an in-plane component and a vertical component that combine to give the total Q factor or

$$Q_{\text{tot}} = \left(\frac{1}{Q_{\text{in plane}}} + \frac{1}{Q_{\text{vertical}}} \right)^{-1} = 2\pi f \frac{U}{P_{\text{in plane}} + P_{\text{vertical}}}, \tag{4}$$

where $P_{\text{in plane}}$ is the power leaving the computational domain over the boundaries vertical to the slab and P_{vertical} is the power leaving through the boundaries parallel to the slab. $Q_{\text{in plane}}$ describes the optical confinement in the plane and is primarily a function of the number of rows of holes in the slab. It can always be increased by increasing the number of

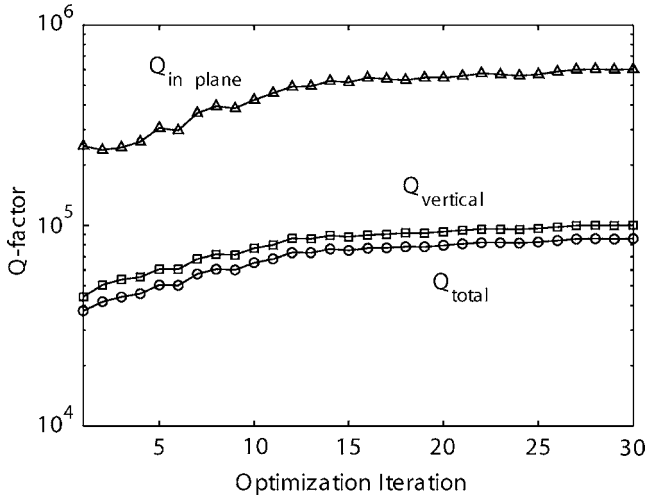

FIG. 8. The improvement in Q_{tot}, Q_{vertical}, and $Q_{\text{in plane}}$ during the optimization. The improvement in Q_{vertical} drives the improvement in Q_{tot}.

rows of holes. Q_{vertical} is primarily a function of the hole pattern immediately in the vicinity of the cavity and the strength of the dielectric-air interface and is thus not as easy to improve.

Since $Q_{\text{in plane}}$ is trivial to improve by adding additional rows of holes, the optimization should primarily address Q_{vertical}. Q_{tot}, $Q_{\text{in plane}}$, and Q_{vertical} are plotted in Fig. 8 for the initial design and during the optimization. For the initial design, Q_{vertical} is much less than $Q_{\text{in plane}}$; thus, improving Q_{vertical} will lead to a greater improvement in Q_{tot} than improving $Q_{\text{in plane}}$. Although in the course of the optimization done here both quantities are improved, the improvement in Q_{tot} is due primarily to the improvement in Q_{vertical}.

Figure 9 shows the intermediate designs as the total reflectivity is increased. The initial round hole becomes trapezoidal and eventually approaches the converged shape. During the optimization, a sharp point exists on the boundary along the plane of symmetry. This sharp point eventually disappears. There is no explicit constraint in the GPM that enforces smoothness at the boundary of the domain, but the boundaries eventually become smooth as a consequence of the optimization. The optimized design does not exhibit any very sharp features that cannot be fabricated.

The correlation between the Q factor and total reflectivity is shown in Fig. 11 as a function of optimization iteration. The Q factor trend does not perfectly match the reflectivity trend but the two curves exhibit the same positive change. Since these data are generated using the verification model discussed above, there is about a 10% uncertainty to each data point. This is apparent in that the initial design, as defined via the GPM, has a Q factor of $\approx$38 000, while the same design, defined as a set of perfect circles using the NURBS surface definition, has a Q factor of $\approx$41 000.

Two conclusions can be drawn from Figs. 9 and 10. The first few iterations appear almost identical, yet they have significantly different Q factors. This implies that the initial design is very sensitive to small changes in the shape of the material boundaries. This is not surprising since Fig. 2 already showed that the Q factor is a strong function of nearest neighbor hole radius. The round holes used in the conven-

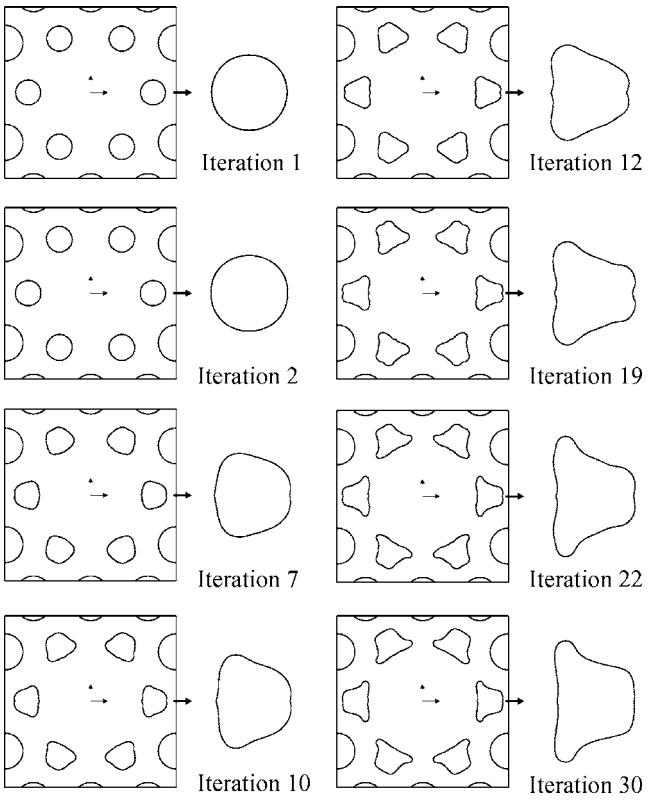

FIG. 9. The intermediate designs during the optimization. The initial nearest neighbor hole shape is shown in gray.

tional approach are clearly a bad choice, as they are highly sensitive to small changes. The design optimized by the GPM, on the other hand, does not exhibit this problem. The last few iterations of the GPM show the opposite trend: relatively large changes in hole shape have only a negligible effect on the Q factor. This leads to the conclusion that the optimal design found via the GPM is more resistant to fabrication defects than the initial design found by the parameter search. This point is particularly important for practical applications of the design method since fabrication by etching or other means may introduce some variation in feature size or shape. Experimental verification of the robustness of the optimized designs is currently underway and will be reported in a future publication.

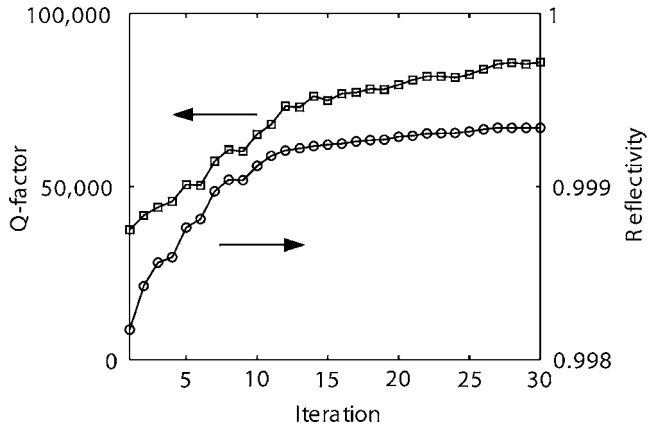

FIG. 10. The improvement in Q factor and reflectivity per optimization iteration. The two curves approximately follow each other.

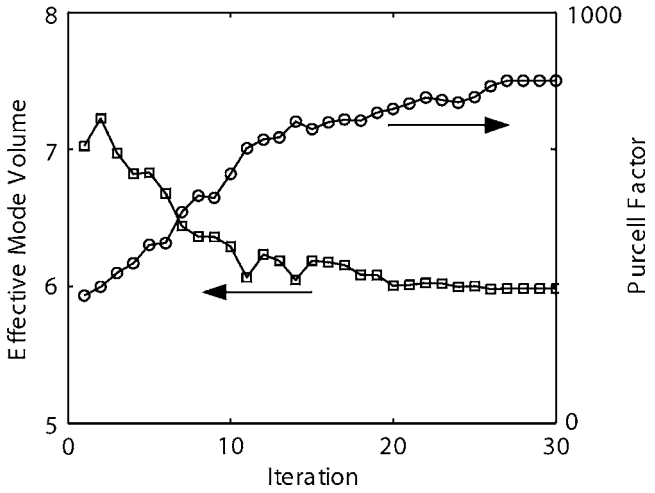

FIG. 11. Effective mode volume and Purcell factor of the lasing cavity during the optimization.

Lastly, the effective volume of the lasing cavity is shown in Fig. 11 as a function of optimization iteration. The effective volume is decreased from about $7(\lambda/2n)^3$ to $6(\lambda/2n)^3$. This decrease in effective volume, although desirable, is unrelated to the optimization objective. The total reflectivity of the structure has no relation to the effective volume. The Purcell factor, which is proportional to the ratio of Q factor to the effective mode volume, is also plotted: it almost triples, from about 300 to 800. It is again stressed that this improvement is not a direct outcome of the optimization problem statement but is nonetheless a positive result.

SUMMARY

In summary, the GPM is used here to improve the Q factor of a photonic crystal laser cavity by optimizing the total structural reflectivity. Initial optimization using a conventional approach is used to find the best combination of nearest neighbor hole radius and surrounding hole radius. The relationship between the total reflectivity of the structure and the Q factor is demonstrated. The GPM is used to improve the total reflectivity, which leads to an improvement in Q factor. The Q factor of the optimized design is more than doubled when compared to the initial design. The designs are verified via models based on the level set curves implicitly defined in the GPM. This work demonstrates one way to optimize the Q factor of a PCL by altering the hole shape.

ACKNOWLEDGMENTS

The support of NSF Grant No. ECS-05-08473 is gratefully acknowledged.

[1] O. Painter, R. K. Lee, A. Scherer, A. Yariv, J. D. O'Brien, P. D. Dapkus, and I. Kim, Science **284**, 1819 (1999).
[2] H. Yokoyama, Science **256**, 66 (1992).
[3] K. Vahala, Science **424**, 839 (2003).
[4] H. Y. Ryu, H. G. Park, and Y. H. Lee, IEEE J. Sel. Top. Quantum Electron. **8**, 891 (2002).
[5] H. G. Park, J. K. Hwang, J. Huh, H. Y. Ryu, Y. H. Lee, and J. S. Kim, Appl. Phys. Lett. **79**, 3032 (2001).
[6] H. G. Park, J. K. Hwang, J. Huh, H. Y. Ryu, S. H. Kim, J. S. Kim, and Y. H. Lee, IEEE J. Quantum Electron. **38**, 1353 (2002).

[7]H. G. Park, S. K. Kim, S. H. Kwon, G. H. Kim, S. H. Kim, H. Y. Ryu, S. B. Kim, and Y. H. Lee, IEEE Photon. Technol. Lett. **15**, 1327 (2003).
[8]H. Y. Ryu, M. Notomi, G. H. Kim, and Y. H. Lee, Opt. Express **12**, 1708 (2004).
[9]M. Shirane, S. Kono, J. Ushida, S. Ohkouchi, N. Ikeda, Y. Sugimoto, and A. Tomita, J. Appl. Phys. **101**, 073107 (2007).
[10]J. Huh, J. K. Hwang, H. Y. Ryu, and Y. H. Lee, J. Appl. Phys. **92**, 654 (2002).
[11]K. Hennessy, C. Hogerle, E. Hu, A. Badolato, and A. Imamoglu, Appl. Phys. Lett. **89**, 041118 (2006).
[12]J. Vuckovic, M. Loncar, H. Mabuchi, and A. Scherer, IEEE J. Quantum Electron. **38**, 850 (2002).
[13]A. Rodriguez, M. Ibanescu, J. D. Joannopoulos, and S. G. Johnson, Opt. Lett. **30**, 3192 (2005).
[14]J. Chaloupka, J. Zarbakhsh, and K. Hingerl, Phys. Rev. B **72**, 085122 (2005).
[15]D. Chang, J. Scheuer, and A. Yariv, Opt. Express **13**, 9272 (2005).
[16]P. T. Lee, T. W. Lu, F. M. Tsai, and T. C. Lu, Appl. Phys. Lett. **89**, 231111 (2006).
[17]K. Svanberg, Int. J. Numer. Methods Eng. **24**, 359 (1987).
[18]J. Norato, R. Haber, D. Tortorelli, and M. P. Bendsoe, Int. J. Numer. Methods Eng. **60**, 2289 (2004).
[19]W. R. Frei, D. A. Tortorelli, and H. T. Johnson, Opt. Lett. **32**, 77 (2007).
[20]J. Jin, *The Finite Element Method in Electromagnetics* (Wiley-IEEE, New York, 2002).
[21]M. P. Bendsoe and O. Sigmund, *Topology Optimization* (Springer, New York, 2004).
[22]S. Adachi, J. Appl. Phys. **53**, 8775 (1982).
[23]J. T. Veredeyen, *Laser Electronics* (Prentice Hall, 1994).